

## THE X-RAY BINARY POPULATION IN M33. II. X-RAY SPECTRA AND VARIABILITY

H.-J. GRIMM, J. McDOWELL, A. ZEAS, D.-W. KIM, AND G. FABBIANO  
Harvard-Smithsonian Center for Astrophysics, 60 Garden Street, Cambridge, MA 02138  
Received 2006 August 8; accepted 2007 April 24

### ABSTRACT

In this paper we investigate the X-ray spectra and X-ray spectral variability of compact X-ray sources for 3 *Chandra* observations of the Local Group galaxy M33. The observations are centered on the nucleus and the star-forming region NGC 604. In the observations, 261 sources have been detected. For a total of 43 sources the number of net counts is above 100, sufficient for a more detailed spectral fitting. Of these sources, 25 have been observed in more than one observation, allowing the study of spectral variability on timescales of  $\sim$ months. A quarter of the sources are found to be variable between observations. However, except for two foreground sources, no source is variable within any observation above the 99% confidence level. Only six sources show significant spectral variability between observations. A comparison of  $N_{\text{H}}$  values with H I observations shows that X-ray absorption values are consistent with Galactic X-ray binaries and most sources in M33 are intrinsically absorbed. The pattern of variability and the spectral parameters of these sources are consistent with the M33 X-ray source population being dominated by X-ray binaries: Two-thirds of the 43 bright sources have spectral and timing properties consistent with X-ray binaries; we also find two candidates for supersoft sources and two candidates for quasi-soft sources.

*Subject headings:* galaxies: individual (M33) — Local Group — X-rays: binaries

*Online material:* color figures, extended figure set

### 1. INTRODUCTION

M33 is a late-type spiral galaxy, Sc II–III, and the third largest galaxy in the Local Group. It is a unique galaxy in the Local Group since morphologically it is of intermediate type between the large early-type spiral galaxies and the numerous dwarf galaxies. Other galaxies of this type cannot be investigated with the same depth even with *Chandra*. At a distance of 840 kpc (Freedman et al. 1991) from the Milky Way (MW) M33 is the second nearest major galaxy. It spans roughly  $73' \times 45'$  on the sky. The line-of-sight absorption column density is small,  $N_{\text{H}} \sim 6 \times 10^{20} \text{ cm}^{-2}$  (Stark et al. 1992). M33 is more actively star forming than either the MW or M31 (Hippelein et al. 2003), particularly compared to its much smaller mass.

M33 has been studied with every X-ray mission since *Einstein* (Markert & Rallis 1983), but only recently have high angular resolution and high-sensitivity instruments like *Chandra* and *XMM-Newton* allowed us to study the X-ray source population in depth. Grimm et al. (2005) and Pietsch et al. (2004) have provided source lists and fluxes for the X-ray source population in M33, from the *Chandra* and *XMM-Newton* observations, respectively. In this paper we follow up on the Grimm et al. (2005) *Chandra* survey and present an analysis of the X-ray spectra and variability behavior of X-ray sources in M33. Apart from fluxes, variability and spectral energy distributions are an important diagnostic tool for understanding the emission mechanism(s) in X-ray sources and for classifying these sources. Moreover, spectral and time variability are the main characteristics of X-ray binaries, as shown by the detailed work done for X-ray binaries in the Milky Way (see, e.g., van der Klis 2005).

The paper is organized as follows. In § 2 we describe the data processing, followed in § 3 by the analysis procedures. The results and their implications for the nature of the X-ray source population in M33 are discussed in § 4; we also discuss individual bright sources in detail in § 4.4. We conclude with a summary of the results in § 5. The figures showing the results for the spectral analysis for sources with more than one observation are shown in Appendix B.

### 2. DATA

M33 has been observed with the ACIS instrument on *Chandra* four times (see Grimm et al. 2005). In this paper we use three observations whose ObsIDs and dates are given in Table 1. Due to its angular extent the observed parts of M33 cover all active chips, the standard ACIS-S configuration for ObsID 786, and the standard ACIS-I configuration for ObsID 1730 and ObsID 2023. There is considerable overlap between the different observations. However, due to the decreasing resolution/sensitivity with increasing off-axis angle only the inner part of M33 ( $\sim 8' - 10'$ ) has a significant number of sources in two observations, 786 and 1730. A fourth observation, ObsID 787, was disregarded because it was aimed at studying the nucleus and suffers from both high background and small FOV.

The data from the three observations were processed according to the standard data processing procedure with CIAO versions 3.1, including exposure correction. Source detection was performed with *wavdetect* with scales of 1, 2, 4, 8, 10, 12, and 16 in the energy range 0.3–8 keV. The signal detection threshold was set to  $10^{-6}$ . Source regions correspond to the 95% encircled energy area. For more details of the data analysis (see Grimm et al. 2005).

### 3. ANALYSIS

We separate the analysis in three parts, short-term, long-term, and spectral variability. The different methods are discussed in the following subsections. We assume that the variability of individual sources is independent, so there is no correlation between short-term and long-term variability. Because the number of counts observed in a single observation is not very large even for bright sources, we restrict the spectral variability analysis to a comparison between different observations, when applicable.

The nucleus was excluded from the following analysis because it suffers from strong pile-up in two observations.

#### 3.1. Short- and Long-Term Variability

In order to establish short-timescale variability we perform a Bayesian block analysis of the light curves of individual sources.

TABLE 1  
LIST OF ACIS OBSERVATIONS OF M33

ObsID	Date	Aim Point	Duration (ks)
786.....	2000 Aug 30	Nucleus	45
1730.....	2000 Jul 12	Nucleus	45
2023.....	2001 Jul 06	NGC 604	90

A Bayesian block analysis computes the best approximation to the light curve shape in terms of piecewise constant flux levels or blocks. The discriminator between a single flux level for the whole light curve or two flux levels is the ratio of likelihoods of describing a data segment with one or two blocks. In this analysis the algorithm used is iterative. It starts with the whole light curve and subsequently divides it until the likelihood ratio for dividing a light curve segment becomes smaller than a predefined prior, in this case corresponding to  $\sim 99\%$  confidence level. The Bayesian block analysis is particularly suited for burstlike variability. For more details about the principle of Bayesian blocks and the algorithm used in this analysis (see Scargle 1998). The implementation used here is the same as used by the CHAMP project and described in Kim et al. (2004).

Since a Bayesian block analysis uses only the photon arrival times for computation of the blocks, no binning is necessary. Therefore, there is no intrinsic restriction to the number of photons the algorithm is applicable to. Obviously, establishing variability with a certain confidence becomes less likely for fainter sources.

Because a Bayesian block analysis is particularly sensitive to burstlike variability, we also performed a search for periodic variability with the XRONOS v5.21 tool `efsearch`. This analysis did not yield any source with significant short-term variability.

To establish long-timescale variability we use simple Poisson statistics. This is justified because, with the exception of two foreground sources, no source exhibits strong short-term variability. We compare the difference in fluxes between two observations to the quadratically added errors for the fluxes. If a source is undetected in an observation in which it was in the field of view of *Chandra*, we calculate an upper limit to the source flux using an algorithm developed by Kraft et al. (1991). Since the upper limit value already corresponds to the 99% confidence level, for a comparison with a detected flux we compare the  $3\sigma$  error of the detection directly with the upper limit.

### 3.2. Spectra and Spectral Variability

For 43 out of the total 261 sources the number of counts in at least one observation was larger than 100 net counts, which we consider sufficient to attempt spectral fitting. Of these 43 sources, 25 have been observed in at least two observations. For these sources we also compare the spectral properties with time. The spectral fitting was done with XSPEC v11.3.1. Because of the generally low number of counts the fitting was done for all sources with Cash statistics (Cash 1979). At 100 counts we expect only  $\sim 3$  background sources based on the CDF- $N \log N - \log S$  (Alexander et al. 2003), so the vast majority of these sources are likely to belong to M33.

We first fitted the bright sources with two simple absorbed spectral models, power law and bremsstrahlung, to check the validity of our assumptions about the spectral shape of the faint sources that do not have sufficient counts for detailed spectral modeling (see derivation of the X-ray luminosity function in Grimm et al. 2005). The absorption was in one case a free parameter, in the other case it was fixed to the Galactic value. After validating

that the assumptions about the general power-law shape are correct, we proceeded to fit more complex models to the bright sources.

The results of the simple spectral fitting are presented in § 4. Spectra of sources with more than one observation with best-fit values and corresponding confidence contour plots are shown in Appendix B, except for the spectra of M33 X-7 (CXO J013334.1+303210) and M33 X-9 (CXO J013358.8+305004), which are shown in Figures 7 and 8 and will be discussed in § 4.4.

Based on the confidence regions for the fit parameters, shown in Appendix B, only one of the X-ray sources shows significant spectral variability from observation to observation, M33 X-4 (CXO J013315.1+305317). For the other sources in different observations none of the parameters of a source spectrum show changes corresponding to more than 99% confidence level. This is despite the fact that some sources show significant time variability between observations. However, the number of counts available for most sources for fitting is insufficient to determine spectral parameters to an accuracy good enough to compare two observations. Moreover, degeneracies between model parameters complicate the establishing of variability.

Another approach to spectral variability is the use of hardness ratios. These are relatively crude estimators of spectral changes, but because of the smaller number of degrees of freedom compared to a spectral fit can be statistically preferable. We therefore take all sources that were observed in at least two observations, divide each observation in three equally long parts, and construct hardness ratios from these intervals. Because only sources with more than 100 counts are used in this part of the analysis, the separation in three parts still gives sufficient number of counts ( $\geq 20-30$ ) in each time bin for a hardness ratio analysis (Prestwich et al. 2003). Note that ObsID 2023 is roughly twice as long as the other observations. The energy bands used are the same as in Grimm et al. (2005); 0.3–1.0 keV for the soft band, 1.0–2.1 keV for the medium band, and 2.1–8.0 keV for the hard band. The hardness ratios are defined as

$$\text{HR1} = \frac{M - S}{T}, \quad \text{HR2} = \frac{H - M}{T}, \quad (1)$$

where  $S$ ,  $M$ , and  $H$  are the background and exposure corrected counts in the soft, medium, and hard band, and  $T$  represents the corrected counts in the whole energy band. To compare two observations it is important to take into account the different effective areas of the source location in each observation, especially if the source is located on a front-illuminated chip and in another observation on a back-illuminated chip. We compute the effective area of the source in each observation for each energy band. For comparison with the other observations of the source we normalize the effective area in each band by the effective area value of the aim point of ObsID 1730. Note that the choice of the normalization constant is arbitrary. The results are combined for all available observations. The results for all sources that show evidence of variability are shown in Appendix B.

## 4. RESULTS AND DISCUSSION

### 4.1. Short-Timescale Variability

Except for two sources that are foreground Galactic stars, no source presents variability above the 99% confidence level. In Figure 1 we show the results of the Bayesian block analysis for the only two sources that are variable on short timescales. The dotted histograms represent the count rate binned in 400 s intervals. Note that the binning is for plotting purposes only. The green line is the power spectrum of the light curve. The thick solid line is

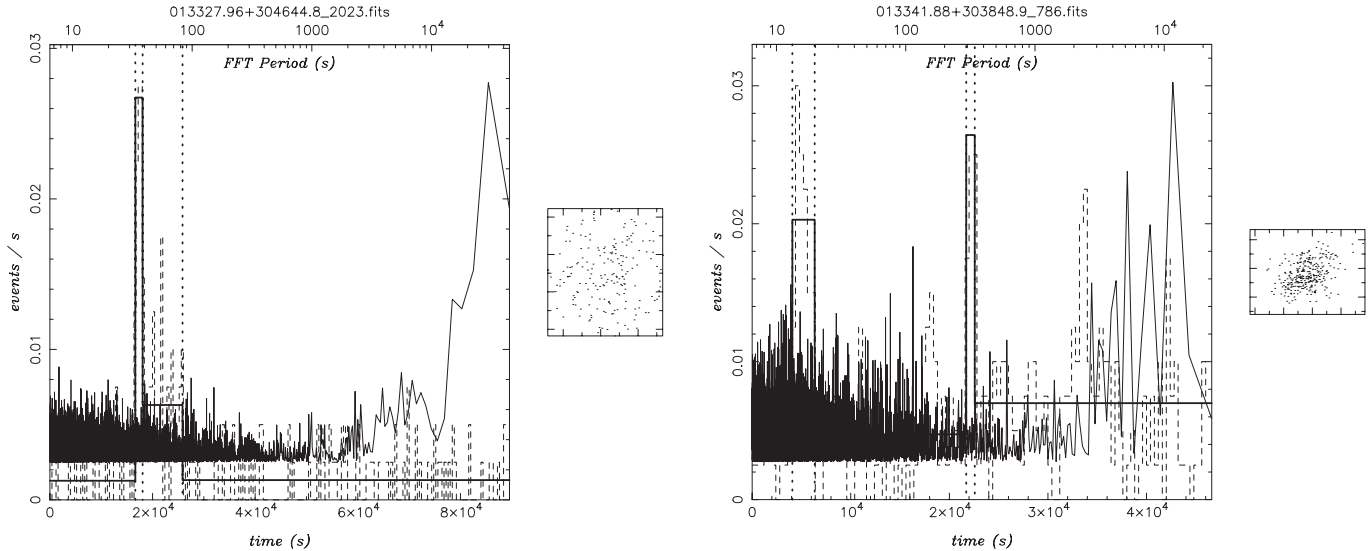


FIG. 1.—*Left*: Light curve and Bayesian block division of the outburst of CXO J013327.7+304645, an X-ray active star. The panel shows the light curve binned in 400 s intervals (*dashed histogram*). Note that the light curve binning is for plotting purposes only. The Bayesian blocks are shown as the thick black histogram. The right part of the panel shows a thumbnail picture of the source. *Right*: Light curve and Bayesian block division of the outburst of CXO J013341.8+303848, another X-ray active star. [See the electronic edition of the Supplement for a color version of this figure.]

the result of the Bayesian block analysis. The small square to the right of the light curve is a thumbnail image of the source from the observation.

Source CXO J013327.7+304645 shows a clear X-ray outburst in ObsID 2023. This outburst, lasting about 10,000 s completely accounts for the long-term variability of the source. The light curve of the outburst is well fitted by an exponential decay with a decay timescale of 3900 s. The persistent luminosity in ObsID 2023 is consistent within the errors with the luminosities in the other observations. Outburst and persistent counts are not large enough to investigate changes in spectral shape. An X-ray color comparison of the burst and persistent emission shows a softening of the emission in HR2 and a slight hardening in HR1 that is significant only at the  $2\sigma$  level. The optical counterpart to source CXO J013327.7+304645 is a star in the USNO catalog with a  $V$  magnitude of 16.8. We have analyzed archival *Hubble Space Telescope* Wide Field Planetary Camera 2 (*HST* WFPC2) data. The object was detected in bands corresponding to  $U$ ,  $B$ ,  $V$ , and  $I$ . The colors are consistent with an early M type star, either on the main sequence or a giant. Using normal  $V$  magnitudes for M stars, this puts the star at a distance of 90–320 pc for a main-sequence star, or 24–29 kpc for a giant. Considering the relatively high Galactic latitude of M33,  $b = -31^\circ$ , the lower distance value, and thus a main-sequence star is more likely. Assuming a main-sequence star the peak luminosity is between  $\sim 10^{29}$  and  $1.5 \times 10^{30}$  ergs  $s^{-1}$ , and the total energy between  $\sim 10^{32}$  and  $1.5 \times 10^{33}$  ergs.

Source CXO J013341.8+303848, a foreground star as well, has two outbursts in ObsID 786. The first outburst lasts about 2600 s, the second outburst 18,000 s later lasts about 800 s. The persistent level of X-ray emission increases slightly after each outburst. As shown in the long-term light curve the source also has a long-term trend to increasing luminosity for the three observations. The decay of the outbursts cannot be fitted uniquely; an exponential decay with a decay constant of  $\sim 1000$  s or a linear decay are both possible. During both outbursts the source becomes softer, but only at the  $1-2\sigma$  level. This source has no *HST* coverage.

#### 4.2. Long-Term Variability

Of a total of 261 sources, 198 have been detected in at least two observations, and 62 in all three observations. The luminosities

for comparison are taken from spectral fits for the brighter sources (more than  $\sim 100$  counts), or from the assumed spectrum, absorbed power law with a photon index of 2 and Galactic absorption. We find that 49 of 198 sources show variability between observations above  $3\sigma$ . An additional 29 sources show signs of variability between 2 and  $3\sigma$ . Of the 49 variable sources, only 16 are apparently persistent.

The strength of the variability can in fact be used to confirm the nature of most of these sources as X-ray binaries. Active galactic nuclei (AGNs) in general show variability on weeks or months timescale only up to factors of 2–3 (Mushotzky et al. 1993; Paolillo et al. 2004). Most of the sources in M33 show stronger variability, particularly since the flux ratios for most sources are only lower limits. Moreover, the sources with flux ratios below 2 are bright sources that are unlikely to be AGNs based only on brightness.

Taking into account that  $\sim 80-90$  of the 198 sources are likely background AGNs, somewhat less than half the sources in M33 are variable. Of these, two-thirds (34/49) may be candidate transients. This number is somewhat higher than the about 50% in the Milky Way and Magellanic Clouds (Liu et al. 2000; Liu et al. 2001). But the detection limits (few  $10^{34}$  ergs  $s^{-1}$ ) do not allow us to establish true transient behavior for undetected sources, so the number of two-thirds is only an upper limit.

For the brighter sources ( $L_X > 5 \times 10^{36}$  ergs  $s^{-1}$ ) past X-ray satellites also provide data for long-term variability. Figure 2 shows data from *Einstein* HRI and IPC (Trinchieri et al. 1988), *ROSAT* HRI (Schulman & Bregman 1995) and PSPC (Long et al. 1996), and *BeppoSAX* (Parmar et al. 2001), as well as from this work for the bright sources in the field of view of *Chandra*. The quoted luminosities are converted to the *Chandra* band of 0.3–8.0 keV and, if they are not individual measurements of spectra, converted to the spectral shape of a power law with photon index of 2 and the Galactic absorption value toward M33,  $6 \times 10^{20}$  cm $^{-2}$ . The error bars in the plot only contain errors due to counting statistics. Other errors, e.g., due to the conversion of energy bands and different assumed spectral shapes, add generally another 20%–30% uncertainty in the luminosity. In addition different instrument responses, cross-calibration issues and other systematic effects add another source of systematic errors, which

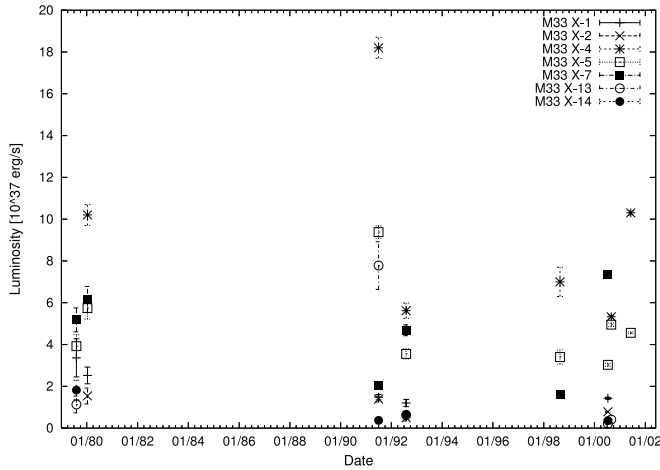


FIG. 2.—Long-term light curves of bright X-ray sources in M33 observed with *Einstein*, *ROSAT*, *BeppoSAX*, and *Chandra*.

is hard to quantify. An exception is the supernova remnant M33 X-14, for which converting the luminosity given by Long et al. (1996) would result in variability at over  $6\sigma$  compared to other observations. However, Long et al. (1996) assume a power-law spectrum with a photon index of 2 to compute the source luminosity. Although this is a reasonable choice for X-ray binaries or AGNs, the spectrum of M33 X-14 is quite soft. We extracted a spectrum of X-14 from the *ROSAT* observation rp600023a00, the longest of the PSPC observations with  $\sim 29$  ks. The spectrum is well fitted by an absorbed blackbody model with a column density of  $4 \times 10^{21} \text{ cm}^{-2}$  and a temperature of 0.09 keV. Although this model is rather unphysical for a SNR we are interested only in the flux, which is sufficiently accurate for the purpose of comparison. The *ROSAT* data also agree with the spectrum obtained from *Chandra*. Extrapolating this spectrum to the *Chandra* energy range gives a luminosity of  $3.7 \times 10^{36} \text{ ergs s}^{-1}$ , which agrees very well with other observations of the source, in particular the *Chandra* observed value of  $3.6 \times 10^{36} \text{ ergs s}^{-1}$ .

It is clear from Figure 2 that four of the bright X-ray sources are variable. The sources that do not show evidence of variability at the  $3\sigma$  level are M33 X-1, X-2, and the SNR X-14.

The variability pattern is very similar to that observed in other X-ray source populations, regardless of galaxy type, e.g., The Antennae (Zezas et al. 2006), M101 (Jenkins et al. 2005), and NGC 4697 (Sivakoff et al. 2005). In particular that only very few, if any, sources show short-term variability is very common, although this is most likely due to limited photon statistics. On the other hand, a large fraction ( $\sim 10\%$ – $40\%$ ) of sources exhibit long-term variability. Moreover, the fraction of sources with strong long-term variability is quite confidently identified as X-ray binaries, and not background AGNs.

### 4.3. Spectra

Fitting all the 43 sources detected with more than 100 net counts with a power-law and a thermal bremsstrahlung spectrum, with column density fixed to the Galactic value or as a free fit parameter, provides about half of the sources with a good fit to the data. The other sources require either different models, e.g., blackbody or other thermal plasma models, or multiple components. The results of the simple power law/bremsstrahlung fits support the validity of our assumptions of a fixed spectral model for conversion from counts to fluxes for fainter sources, assuming that the spectral properties of bright and faint sources are not systematically different (Grimm et al. 2005).

In Figure 3 we show histograms for the best-fit power-law and bremsstrahlung values for all sources. The upper left panel shows the comparison between photon indices  $\Gamma$  of a power law with column density being a free fit parameter versus column density fixed to the Galactic value. The Galactic absorption toward M33 is only  $6 \times 10^{20} \text{ cm}^{-2}$ . The upper right panel shows the same for bremsstrahlung temperature  $kT$ . The lower left panel shows the histogram of  $\Gamma$  for the case of  $N_{\text{H}}$  as a free fit parameter. The power-law slopes are concentrated around 2, the canonical value for X-ray binaries and AGNs. The peak at  $\Gamma = 5$  comprises all sources with photon index larger than or equal to 5. Individually, all these sources are fitted well with a blackbody or plasma model with temperatures of 0.1–0.13 keV (blackbody) or 0.2–0.3 keV (plasma model). The lower right panel finally shows the distribution of bremsstrahlung temperatures. Note that the influence of  $N_{\text{H}}$  is stronger in case of a power law than for a bremsstrahlung spectrum, as is evident in the generally smaller deviations from the one-to-one correlation for the bremsstrahlung temperatures compared to the photon indices in the upper panels.

As expected, fits with a fixed low column density produce smaller photon indices or larger bremsstrahlung temperatures, respectively. However, changes of temperature and photon index between fits with fixed and free column density are not significantly larger than the errors in the majority of cases. Comparing the difference between photon indices divided by the square root of the errors shows that  $\sim 80\%$  of the sources have values of less than 3. For the thermal bremsstrahlung model the corresponding value is 73%. Thus, the assumption of a general power-law spectrum with  $\Gamma = 2$ , and Galactic absorption is quite good (Grimm et al. 2005).

Using the results of the more detailed spectral fitting of the 43 bright sources, we can confirm the results of the relatively blind spectral fitting of all sources with a power-law model. The left panel of Figure 4 shows the photon indices of spectra that are well fitted by either a single power law (*open circles*) or a combination of a power law and other components (*filled triangles*) versus luminosity. Errors are 90% errors on the slope. There is a clear trend that photon indices in multicomponent fits are larger than for single power-law fits, and there is an indication that brighter sources are more likely well fitted by multicomponent fits than by single power laws. The reason is most likely that the single power-law sources have lower counts and multiple components are not distinguishable. We also fit the single power-law sources with a disk blackbody model, XSPEC model *diskbb*, which has the same number of degrees of freedom than the power-law model. Two-thirds of the spectra are well fitted by a disk blackbody model, the best-fit temperatures being in the range from 1 to 3 keV, as expected for X-ray binaries (Tanaka 2001). The inner disk temperatures versus luminosity are shown in the middle panel of Figure 4. The values are the same as for the sources that require disk blackbodies for a good fit. This suggests that the single power-law sources are likely to be X-ray binaries and only the low number of counts allows a good fit with a single power law.

There are 10 spectra (5 sources) that are best fitted with a single bremsstrahlung model with temperatures of  $\sim 0.1$ – $0.3$  keV. The bremsstrahlung temperatures versus luminosity are shown in the right panel of Figure 4 (*open squares*). Since these values are unusually low for real bremsstrahlung sources, and the luminosities of the sources relatively low,  $(1-5) \times 10^{36} \text{ ergs s}^{-1}$ , we fit these spectra with a thermal plasma model (XSPEC model *apex*) as well. With one exception, we obtain good fits with the plasma model as well, the temperatures are in the range from 0.1 to 0.4 keV, and metallicities from 0.05 to 0.3 solar with considerable uncertainties. These values are at or below the expected metallicity for

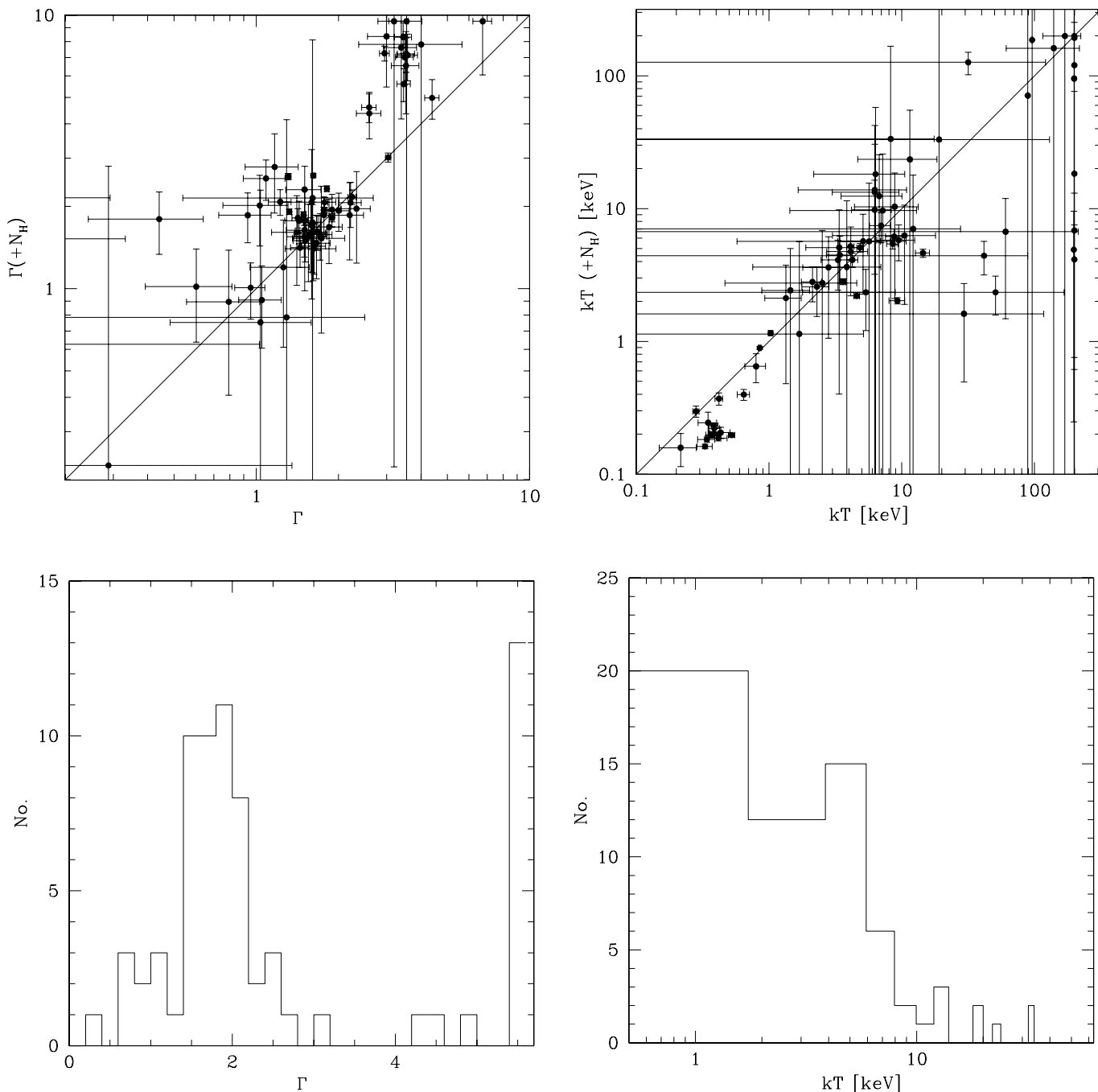


Fig. 3.—Overall spectral properties of the sample of 43 bright X-ray sources in M33. The upper panels show the correlations of photon index  $\Gamma$  with  $N_{\text{H}}$  free vs. fixed (*upper left*) and bremsstrahlung temperature  $kT$  with  $N_{\text{H}}$  free vs. fixed (*upper right*). Note that the influence of  $N_{\text{H}}$  is stronger in case of a power law than for a bremsstrahlung spectrum, as evident in the smaller deviations from the one-to-one correlation for the bremsstrahlung temperature. The lower panels show the distributions of  $\Gamma$  (*lower left*) and  $kT$  (*lower right*) for the case of  $N_{\text{H}}$  as a free fit parameter. The power-law slopes are mainly in the range from 1.4 to 2.5, the canonical values for X-ray binaries and AGNs.

M33 (Blair & Kirshner 1985). The good fit quality is not surprising considering that the *apec* model has one degree of freedom more than the simple bremsstrahlung model. However, given the low temperatures and the consistent metallicities we consider the *apec* model to be the more physical model for these sources. The sources with good fits for the *apec* model are marked in Table 3 (Appendix B), and the *apec* model parameters are given in Figure Set 9 (Appendix B), and the contour plots for these fits are shown as well. Also shown in the right panel of Figure 4 are six sources well fitted by a blackbody model with very low temperatures at or below 0.1 keV (*filled triangles*). For two sources the

blackbody is the only component in the spectrum. These sources are candidates for supersoft sources and are discussed below in § 4.4. Three of the other four sources have an additional power-law component that ranges from hard ( $\Gamma \sim 1.3$ ) to very soft ( $\Gamma \sim 4.6$ ). The blackbody temperatures are even lower than the temperatures inferred from ULX intermediate mass black hole candidates (see, e.g., Miller et al. 2004). A truncated disk would be a possibility to explain the low temperature, similar to the scenario suggested by Kubota & Done (2004). However, given the luminosities the sources would be in the hard state (e.g., Maccarone 2003) but, except for CXO J013444.6+305535, the photon indices

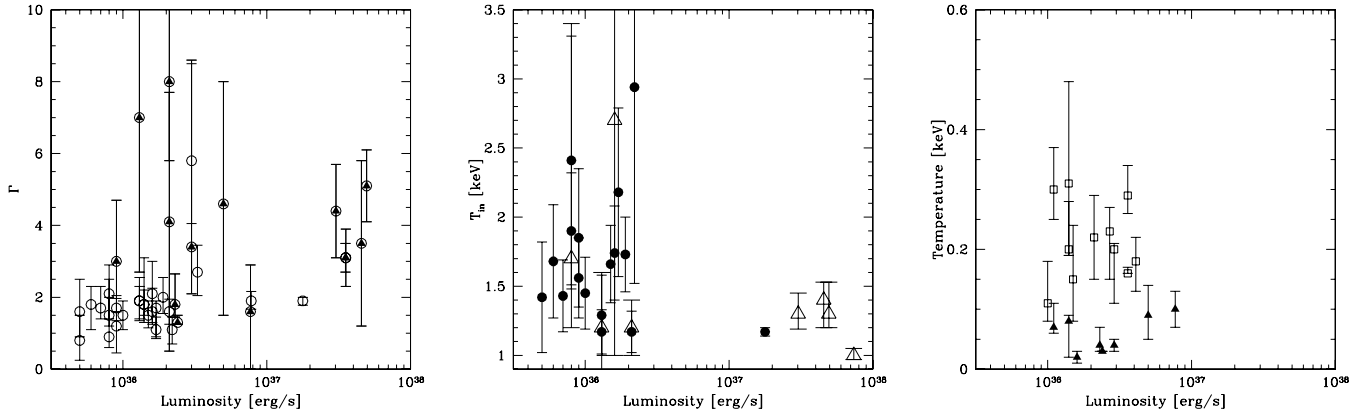


FIG. 4.— Left panel shows the best-fit photon indices for sources that are well fitted by a single power-law (*open circles*) or a multicomponent spectrum containing a power law (*open circles with filled triangles*) vs. luminosity. Two-thirds of the single power-law sources are also well fitted by a disk blackbody model. The middle panel shows the disk blackbody temperatures vs. luminosity for sources that are well fitted by a single power law, but also by a simple disk blackbody model (*filled circles*). As expected for X-ray binaries the disk temperatures are in the range from 1 to 3 keV. The temperatures are also in the same range as the temperatures for sources that require a disk blackbody component in the spectrum (*open squares*) or a blackbody model (*filled triangles*) vs. luminosity. Right panel shows temperatures of sources that are either well fitted by a bremsstrahlung model (*open squares*) or a blackbody model (*filled triangles*) vs. luminosity. With the exception of two spectra, the bremsstrahlung sources are also well fitted by a thermal plasma model, XSPEC model *apec*, as discussed in the text. Errors are at 90% confidence level. [See the electronic edition of the Supplement for a color version of this figure.]

are larger than 2. CXO J013444.6+305535 could indeed be in the hard state with a photon index of 1.3, but that number is not well constrained. This hard source could also be a candidate for a magnetic CV that are known to have hard spectra and relatively high luminosities (Kuulkers et al. 2006). The soft power law in the other sources might on the other hand be another thermal component. Alternatively, the soft emission might be generated in an outflow from the system, or heating of a surrounding medium.

Figure 5 shows a comparison of measured values for column density overlaid on a 1.49 GHz contour map of the central part of M33 from VLA (Condon 1987). The resolution of the VLA map is about  $1'$ , and the confusion limit is given as 0.1 mJy. There is no spatial correlation between the contour map and the magnitude of the measure column densities. Thus, the X-ray absorption value is in part due to location of sources in front of/behind H I gas, and in part due to intrinsic absorption around the X-ray source.

To compare actual values for the column density due to H I, we compute the brightness temperature of the H I gas according to

$$S_\nu = \frac{2k\nu^2\Omega}{c^2} T_b, \quad (2)$$

where  $S_\nu$  is the radio flux in units of Jy  $\text{sr}^{-1}$  at frequency  $\nu$  (1.49 GHz),  $\Omega$  is the opening angle of the beam ( $1'$ ), and  $T_b$  is the brightness temperature;  $k$  is the Boltzmann constant, and  $c$  is the speed of light. Assuming optically thin emission we compute the H I column density according to

$$N_{\text{H}} = 1.83 \times 10^{18} T_b \text{ [K cm}^{-2}\text{]}. \quad (3)$$

Within the size of a beam the radio flux has an rms of  $\sim 5$  mJy around the zero point. Therefore, we take 5 mJy as the upper limit on the sensitivity in a beam. This flux corresponds to  $\sim 320$  K or  $N_{\text{H}}$  of  $5.7 \times 10^{20} \text{ cm}^{-2}$ , which is very close to the Galactic absorption value. Figure 6 shows the comparison between the X-ray absorption values from spectral fitting and the “expected” absorption from H I.

Filled circles are sources in M33, crosses are a selection of Galactic X-ray binaries from Vrtilik et al. (1991). Upper limits are shown as arrows. The vertical and horizontal lines denote the Galactic absorption value. The figure can be separated into roughly

three regions: (1) Sources at or below the horizontal line, i.e., sources with apparently *less* absorption than the Galactic value, which probably have an undetected thermal component in the spectrum; (2) sources below the diagonal line that are probably located in front of at least parts of the H I emission (these sources are most likely on the Milky Way facing side of M33); (3) sources above the diagonal line that are intrinsically absorbed. No conclusion as to their location can be drawn.

Values for Galactic X-ray binaries are taken from Vrtilik et al. (1991) and Liu et al. (2001) for  $A_V$  values missing in the former. We convert the optical extinction to neutral hydrogen column density according to Predehl & Schmitt (1995),  $N_{\text{H}} = 1.77A_V$  in units of  $10^{21} \text{ cm}^{-2}$ , and use  $A_V = 3E(B - V)$  in cases where only the reddening is available. The comparison with Galactic X-ray binaries shows that M33 X-ray sources also often show excess absorption at levels comparable with Galactic X-ray binaries. The larger values for  $N_{\text{H}}(\text{H I})$  in the Milky Way can be explained simply by our location in the Milky Way, compared to the nearly face-on orientation of M33.

Only six of the 25 sources observed in more than one observation with more than 100 counts show significant variability in the hardness ratio diagram (see Appendix B). Three of the sources are the well-known sources, M33 X-4, M33 X-5, and M33 X-13. The other three are CXO J013329.0+304216, CXO J013329.3+304508, and CXO J013410.5+303946. There is a clear separation in that most sources have a very small significance for moving in the hardness ratio diagram, whereas four of the ones that show changes in hardness ratio are above 99.99% confidence level.

Based on spectral shape (photon indices, temperatures) and absorption properties, we conclude that M33 X-ray sources as a population are very similar to Galactic X-ray binaries.

#### 4.4. Individual Sources

Here we discuss the properties of individual bright M33 sources. These include previously known sources (M33 X-...) and sources newly discovered in our *Chandra* observations. Wide-band spectral studies exist in the literature for some of these sources. In particular, *BeppoSAX* has observed the brightest sources in M33 and measured spectra of the sources M33 X-4 to M33 X-10 in the energy range from 2.0 to 10.0 keV (Parmar

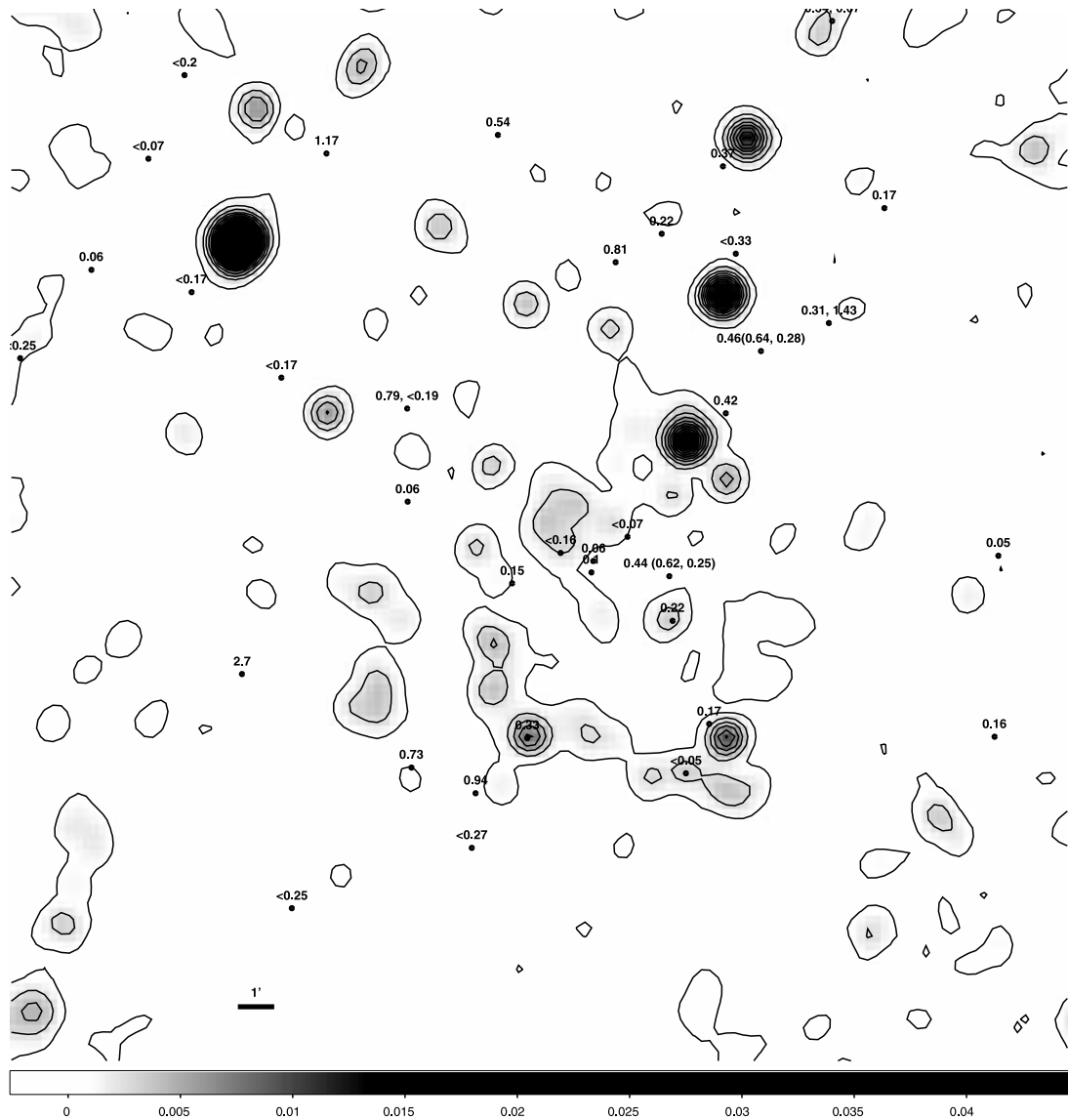


FIG. 5.—Measured values for column density overlaid on a 1.49 GHz contour map of the central part of M33 from VLA (Condon 1987). The resolution of the VLA map is about  $1'$ , and the rms is about 0.1 mJy. Prominently visible is the H II region NGC 604 at the upper left. Also visible toward south of the center is the southern spiral arm. There is no correlation between the contour map and the magnitude of the measure column densities. [See the electronic edition of the Supplement for a color version of this figure.]

et al. 2001). Of these sources, X-6 and X-10 are not in the field of view of the *Chandra* observations, and X-8 is the nucleus, which is not discussed here.

*M33 X-4 (CXO J013315.1+305317)*.—The X-ray spectrum of this soft source measured by *BeppoSAX* is well fitted by either a power-law model with photon index of  $\sim 3$  or a bremsstrahlung model with  $kT \approx 2$  keV. This source has been observed by *Chandra* twice, in ObsID 786 and ObsID 02023. Between the observations, the flux increased by a factor of 2 from  $5 \times 10^{37}$  to  $10^{38}$  ergs  $s^{-1}$ . The variability rules out the interpretation of the source as a SNR (Okada et al. 2001). Using the overlapping energy range with the *BeppoSAX* observations, 2.0–8.0 keV, we obtain the same values for absorption, photon index, and bremsstrahlung temperature well within the errors and  $\chi^2$ -values below 1 for observation 786. For observation 2023, although the best-fit values are consistent with the *BeppoSAX* and ObsID 786 values, the  $\chi^2$ -values are well above 2. Moreover, for the whole *Chandra* range, 0.3–8.0 keV, none of these models is a good fit. A statistically satisfactory fit for both ObsIDs can be achieved

with a model consisting of a blackbody and a power law. The blackbody temperatures ( $\sim 0.65$  keV) and photon indices (3–4.7) for the two observations are consistent within the errors. However, the absorption to the source changes. Taking into account the different values for absorption there is a clear distinction at 99% confidence level in the contour plots, for  $\Gamma$  versus  $N_H$  and  $kT$  versus  $N_H$ . The difference in  $\Gamma$  versus  $kT$  is significant only at 90% confidence level. The blackbody temperature is relatively low and does not change significantly, but similar values for disk blackbody temperatures have been observed in Galactic BHs. These temperatures occur at luminosities of  $\sim 1\%$ – $5\%$  of the Eddington luminosity (Gierliński & Done 2004). With a luminosity increasing from  $\sim 5 \times 10^{37}$  to  $10^{38}$  ergs  $s^{-1}$ , this interpretation would make the compact object in X-4 a rather massive but still stellar mass BH given the luminosity. The photon index of the power-law component is much softer than expected for a low-hard state black hole (Tanaka 2001) but is in agreement with high-soft state Galactic black holes (McClintock & Remillard 2006). The change in the photon index between the observations

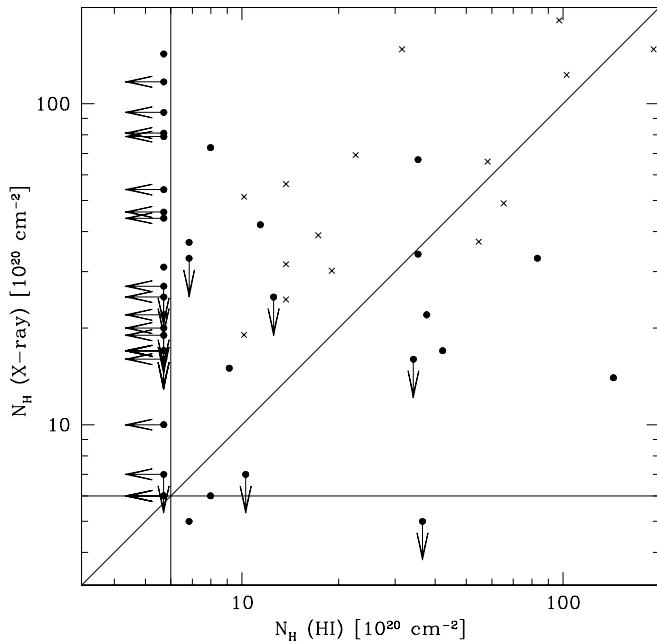


FIG. 6.— Measured values for column density from X-ray spectral fitting vs. absorption values inferred from H I radio flux. Upper limits are shown as arrows. Vertical and horizontal lines denote the Galactic absorption value. Filled circles are sources in M33, crosses are Galactic X-ray binaries, see text. The plot can be separated into three regions: (1) At or below the horizontal line, sources with apparently less absorption than the Galactic value; (2) below the diagonal line, sources are probably located in front of at least parts of the H I emission; (3) above the diagonal line, sources are also intrinsically absorbed. [See the electronic edition of the Supplement for a color version of this figure.]

(from  $\sim 3$  to 4.7) does not indicate a state change from low-hard to high-soft. Even a photon index of 3 is too large for the low-hard state ( $\Gamma \sim 1.7$ ). The photon index is also in the range observed for the Galactic XRB Sco X-1, which has a neutron star primary (Bradshaw et al. 2003), but Sco X-1 does not exhibit a soft component like M33 X-4 (Kahn et al. 1984). Thus, based on the X-ray data the source is likely to be a BH binary.

The hardness ratio analysis shows that the hardness of the source varies significantly between the observations. The source becomes harder in HR1 and softer in HR2, while the luminosity increases by a factor of  $\sim 2$ . This change is due to the increase in the medium band (1.0–2.1 keV) with respect to the soft and hard band, which is reflected in the spectral fits by a higher absorption column and a lower power-law photon index.

*M33 X-5 (CXO J013324.4+304401).*—This source has been observed in all three *Chandra* observations. For M33 X-5 (CXO J013324.4+304401) *BeppoSAX* as well finds good fits with a soft power-law ( $\Gamma \approx 3$ ) or bremsstrahlung model ( $kT \approx 2.8$  keV). In all *Chandra* observations the overlapping energy range is fitted satisfactorily with these values. However, for the whole *Chandra* energy range neither a single power-law nor a bremsstrahlung spectrum give good fits. A good fit is obtained with a disk blackbody ( $\sim 1.3$  keV) and power-law ( $\Gamma = 4$ –9) combination. The contour plots in Figure Set 9 (Appendix B) show no significant variation of the spectral parameters given the large uncertainties. The errors on the photon index are large enough to not make the changes between observations significant. However, a disk blackbody alone does not yield a good fit. The disk blackbody temperature is in good agreement with observations of Galactic BH binaries at moderately sub-Eddington luminosities (Gierliński & Done 2004). The luminosity of the sources changes between  $3 \times 10^{37}$  and  $5 \times 10^{37}$  ergs  $s^{-1}$ ; thus, it is significantly below the

Eddington limit for a black hole but in the range of transition luminosities from the low-hard to the high-soft state of Galactic black holes (Maccarone 2003). Another interpretation is that the source is a neutron star and the steep power law corresponds to the harder thermal component from the neutron star surface (Tanaka 2001). Due to the complexity of the combined model only the disk temperature is well determined.

However, the hardness ratio analysis shows significant variation between ObsIDs 1730 and ObsID 786 on the one hand and ObsID 2023 on the other. X-5 becomes significantly softer in HR1 but does not change significantly in HR2. There seems to be no correlation with luminosity as ObsIDs 786 and 2023 have the same luminosity but significantly different HR1 values.

*M33 X-7 (CXO J013334.1+303210).*—This source has been observed only in *Chandra* observation 1730. For M33 X-7 (CXO 013334.1+303210) *BeppoSAX* as well finds good fits with a power-law ( $\Gamma \approx 2$ –3) or bremsstrahlung model ( $kT \approx 3.7$  keV). In the 2.0–8.0 keV energy range both models provide satisfactory (power law) to good (bremsstrahlung) fits to the *Chandra* data. The photon indices for fixed and variable absorption are larger than in the *BeppoSAX* observations but still within the rather large errors. The bremsstrahlung temperatures for fixed and variable absorption are smaller, and in the case of fixed absorption inconsistent with the lower limit of the *BeppoSAX* observation. Although the errors are quite large this indicates that the source was softer in the *Chandra* observations. Moreover, M33 X-7 was about 5 times brighter in the *Chandra* observation ( $\sim 7 \times 10^{37}$  ergs  $s^{-1}$ ) compared to the time *BeppoSAX* observed the source ( $\sim 1.6 \times 10^{37}$  ergs  $s^{-1}$ ) (note that both luminosities are based on spectral fits). The only satisfactory fit to the whole energy range of *Chandra* is an absorbed disk blackbody with an inner disk temperature of  $1 \pm 0.02$  keV. This value is consistent with inner disk temperatures of Galactic black holes (McClintock & Remillard 2006). The column density is not well constrained, but below  $6.5 \times 10^{20}$   $cm^{-2}$ , putting the upper limit of the absorption at the Galactic value. Pietsch et al. (2004) obtain the same values within the errors for an *XMM-Newton* observation, and also new *Chandra* observations give the same spectral parameters (Pietsch et al. 2006). This might indicate the presence of an additional soft component that due to insufficient counts presents itself as a low absorption value. An additional soft component, however, does not improve the fit, and its parameters are not well determined. Figure 7 shows the spectrum and the contour plot of absorption column density versus inner disk temperature. Given the softer spectrum in the *Chandra* observation, a possible additional soft component, and the 5 times higher luminosity, it is possible that X-7 underwent a state transition. On the other hand, the photon index of the power law in the *BeppoSAX* spectrum is already softer than expected for a low-hard state source (Tanaka 2001).

*CXO J013343.4+304630 and CXO J013409.9+303219.*—These sources are the best candidates for supersoft sources (SSS) in M33. CXO J013343.4+304630 is well fitted by a blackbody spectrum with a temperature of about 75 eV and moderate absorption ( $N_H \sim 8 \times 10^{21}$   $cm^{-2}$ ). The source shows no significant spectral variability but is variable on timescales of months. CXO J013409.9+303219 has been observed only once. Its spectrum is also well fitted by a blackbody with a temperature of 37 eV and also moderate absorption ( $N_H \sim 7 \times 10^{21}$   $cm^{-2}$ ). The temperatures are in the range for SSSs, and the sources are not significantly detected above 1 keV (see, e.g., Kahabka & van den Heuvel 1997). Given their luminosities of  $\sim (3$ – $10) \times 10^{35}$  ergs  $s^{-1}$  (CXO J013343.4+304630) and  $\sim 3 \times 10^{36}$  ergs  $s^{-1}$  (CXO J013409.9+303219) these sources are most likely nuclear burning white dwarfs.

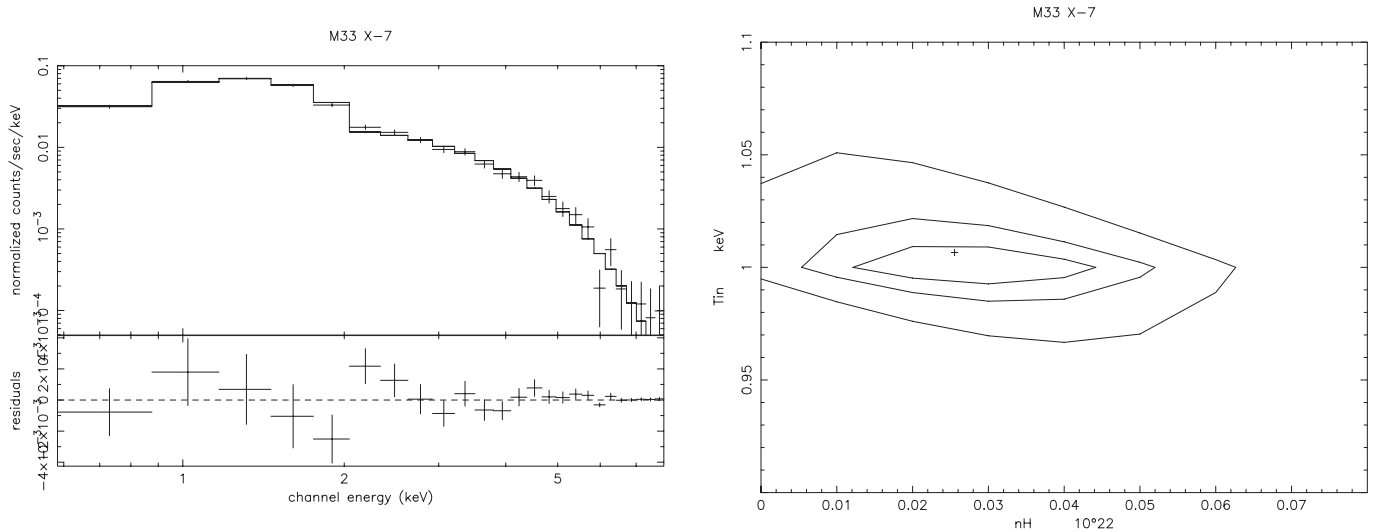


Fig. 7.—Energy spectrum and contour plot for M33 X-7. The model spectrum is an absorbed disk blackbody with an inner disk temperature of  $1 \pm 0.02$  keV and  $N_{\text{H}} < 6.5 \times 10^{20}$  cm $^{-2}$ . The reduced  $\chi^2$  is 1.2. [See the electronic edition of the Supplement for a color version of this figure.]

*M33 X-9 (CXO J013358.8+305004)*.—This source was observed in *Chandra* observations 786 and 2023. It is well fitted by a power law with photon index of  $\sim 1.2$  in the *BeppoSAX* observation. For a bremsstrahlung model only lower limits to the temperature are provided ( $>2.6$  keV). It is important to note that in the *BeppoSAX* observations X-9 is unresolved, but *ROSAT* observations have shown that X-9 actually consists of 3 sources, at least two of which seem to be variable and of comparable flux (Long et al. 1996). Since *BeppoSAX* does not resolve the sources, it is impossible to say whether any of them dominate the spectrum and, if yes, which one. The *Chandra* source is associated with the source X-9a based on the *ROSAT* position. In the whole *Chandra* energy range a power law is a good fit. The absorption column is not well constrained in this fit, but the values for the photon index are  $\sim 1.7$ , with a reduced  $\chi^2$  of 0.87. Figure 8 shows the spectrum and the contour plot of absorption column density versus photon index. Assuming for the sake of the argument that a significant fraction of the *BeppoSAX* flux originated from X-9a, the source was thus significantly harder during the *BeppoSAX* observation. Even if there is no spectral change in X-9, the source was then about a factor of 10 brighter during the *ROSAT* observations where

it reached  $\sim 1.4 \times 10^{37}$  ergs s $^{-1}$ . Between the two *Chandra* observations the source luminosity decreases by a factor of  $\sim 2$  from  $1.7 \times 10^{36}$  to  $7 \times 10^{35}$  ergs s $^{-1}$  without a significant change in spectral parameters. Based on the variability, either spectral and/or timing, and the luminosity the source is thus highly likely to be an X-ray binary.

*M33 X-13 (CXO J013354.8+303309 and CXO J013329.0+304216)*.—These two sources have very soft bremsstrahlung temperatures ( $\sim 0.2$  keV) but are also variable on timescales of months, thus excluding SNRs or H II regions as counterparts.

*M33 X-13 (CXO J013354.8+303309)* is well fitted with a bremsstrahlung model with temperature 0.22 keV and absorption of  $\sim 3 \times 10^{21}$  cm $^{-2}$  in both observations. The source is coincident with a SNR (Gordon et al. 1999), but the flux varies by a factor of 2 between two observations. It also shows significant change in the hardness ratios. The source becomes softer in HR1 and harder in HR2. The flattening of the spectrum is accompanied by an increase in luminosity from  $2 \times 10^{36}$  to  $4 \times 10^{36}$  ergs s $^{-1}$ .

CXO J013329.0+304216 shows a significant softening in HR1 and hardening in HR2 from ObsID 1730 to ObsID 2023, the same behavior at similar hardness ratios like M33 X-13

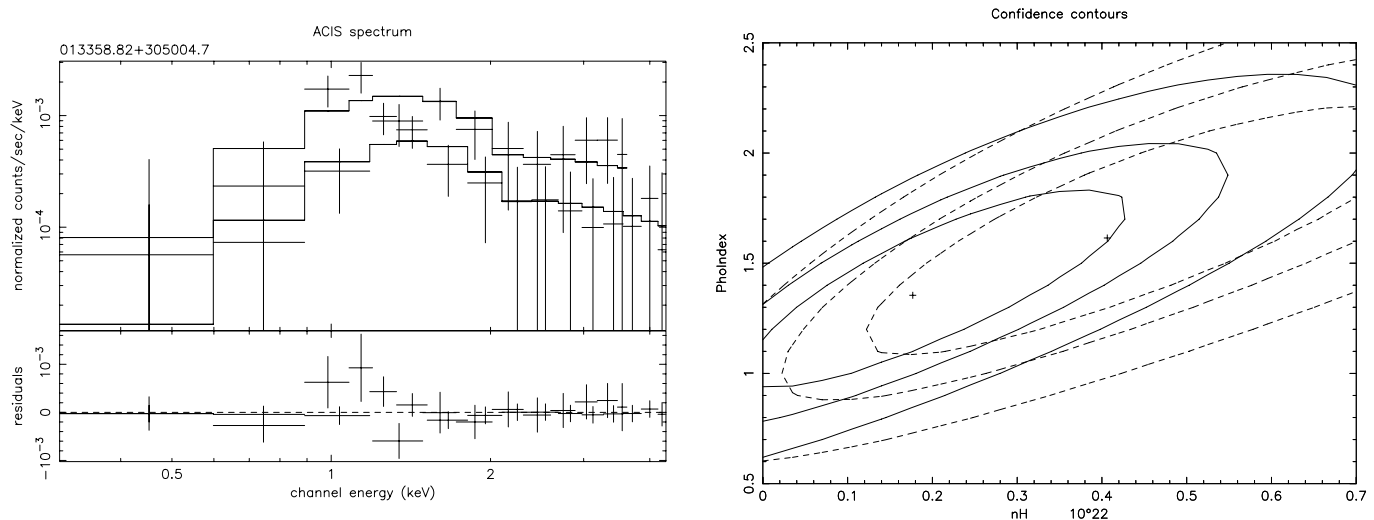


Fig. 8.—Energy spectrum and contour plot for M33 X-9. The model spectrum is an absorbed power law with a photon index of  $1.88 \pm 0.04$ . The reduced  $\chi^2$  is 0.87. [See the electronic edition of the Supplement for a color version of this figure.]

(CXO J013354.8+303309). The spectrum of the source is well fitted by a bremsstrahlung spectrum with a temperature decreasing from  $0.24 \pm 0.01$  keV (ObsID 1730) to  $0.21 \pm 0.006$  keV (ObsID 786) and to  $0.19 \pm 0.006$  keV (ObsID 2023). However, the temperature is somewhat degenerate with the column density, which increases from  $(0.29 \pm 0.1) \times 10^{-22}$  cm<sup>-2</sup> (ObsID 1730) to  $(0.36 \pm 0.1) \times 10^{-22}$  cm<sup>-2</sup> (ObsID 786) and to  $(0.42 \pm 0.17) \times 10^{-22}$  cm<sup>-2</sup> (ObsID 2023). Although the column density changes systematically, the large errors make it impossible to choose which, if any, value is correct. Thus, although the errors on the temperatures are small the significance of the temperature change from the spectral fit is not large. Between the *Chandra* observations the luminosity increases from  $2.7 \times 10^{36}$  to  $3.6 \times 10^{36}$  ergs s<sup>-1</sup>.

Temperature and variability of these sources indicate that they could be quasi-soft sources, although a simple blackbody does not provide a good fit. However, more complicated models (e.g., blackbody plus power law) do not improve the fits due to the small number of observed counts. For quasi-soft sources the luminosities would be relatively low (a few  $10^{36}$  ergs s<sup>-1</sup>) but still in the range observed in other galaxies (Di Stefano & Kong 2004). The sources are too bright [ $\sim(2-4) \times 10^{36}$  ergs s<sup>-1</sup>] for normal CVs ( $\sim 10^{30}-10^{32}$  erg s<sup>-1</sup>), and magnetic CVs that can reach such luminosities have very hard spectra with effective temperatures of several keV (Kuulkers et al. 2006). On the other hand, the sources have too high temperatures for supersoft sources (Kahabka & van den Heuvel 1997).

*CXO J013329.3+304508 and CXO J013410.5+303946.*—The two sources show evidence for spectral variability in their hardness ratio diagrams. Source CXO J013329.3+304508 shows a significant softening in HR1 but no change in HR2 from ObsID 1730 to ObsID 2023. The best-fit model for the spectrum is a bremsstrahlung model; however, the temperature is not well determined in the fit. Moreover, the source is variable between ObsIDs 786 and 2023, between which the luminosity decreases by  $\sim 30\%$  from  $3 \times 10^{36}$  to  $2 \times 10^{36}$  ergs s<sup>-1</sup>. Source CXO J013410.5+303946 shows a softening in HR1 from ObsID 1730 to ObsID 786 but no significant change in HR2. From ObsID 786 to ObsID 2023 the HR1 hardens again so that the hardness ratio for ObsID 2023 is consistent with the hardness ratio for ObsID 1730. The spectrum of ObsIDs 1730 and 2023 is well fitted by a disk blackbody with an inner disk temperature 1.2 keV. The spectrum of ObsID 786 on the other hand is well fitted by a power law with a photon index of 1.7. Both photon index and disk temperatures are consistent with Galactic X-ray binary spectra (Tanaka 2001). It is interesting to note that the luminosity increases between the first two observations and stays high in the third, although the spectral shape in the first and third observation are basically identical. The source increased its luminosity between ObsIDs 1730 and 786 from  $\sim 1.3 \times 10^{36}$  to  $\sim 2.1 \times 10^{36}$  ergs s<sup>-1</sup> and had the same high luminosity during ObsID 2023. Although the power-law spectrum is relatively hard, the softening of the hardness ratio and the increasing luminosity do not indicate a state change in the system.

The spectral and timing behavior of the bright X-ray sources in M33 is varied but can be well described within the framework of Galactic X-ray sources and X-ray sources in other galaxies observed with *Chandra*.

## 5. SUMMARY AND CONCLUSION

In the three *Chandra* observations of M33, performed between the years 2000 and 2001, 261 sources have been detected in the range of X-ray luminosities from  $L_X \sim 10^{34}-10^{38}$  ergs s<sup>-1</sup>

(0.3–8.0 keV). Of this total, 198 sources have been detected in at least two observations, and 62 sources have been observed in all three observations. We find that 49 sources show variability between observations above  $3\sigma$ . For a total of 43 sources, 25 of which in more than one observation, the number of counts is sufficient for a more detailed spectral fitting. Given the angular extent of our survey we expect  $\sim 3-4$  AGN interlopers for sources with luminosities above  $10^{36}$  ergs s<sup>-1</sup>, and about one for sources with luminosities above  $10^{37}$  ergs s<sup>-1</sup> (see Grimm et al. 2005). All sources in M33, except for the nucleus, have luminosities below  $\sim 10^{38}$  ergs s<sup>-1</sup>.

*Time variability.*—Roughly a quarter (49/198) of all *Chandra* sources exhibits long-timescale variability ( $\sim$ weeks–years); therefore, we can exclude SNRs and H II regions in M33 as their counterparts. Except for two Galactic star interlopers none of the M33 sources show any short-timescale X-ray variability ( $\sim$ seconds to hours). Detection of such variability would separate stellar mass objects from AGNs, since in AGNs the light travel time is too large to produce variability on timescales shorter than hours. However, the amplitude of the long-term variability (larger than a factor of 2–3) makes it unlikely for the variable sources to be AGNs (generally less than a factor of 2–3).

A significant number of sources showing long-term variability but little to no short-term variability is very similar to other extragalactic X-ray source populations. The comparison of the amplitude of long-term variability with AGNs and known X-ray binaries shows that a large majority of these sources are X-ray binaries.

*X-ray spectra.*—The large majority of source spectra is well fitted by models containing either a power law or a thermal plasma (bremsstrahlung or apec), but in the most luminous sources more complex models are required. Of the 43 sources with enough counts for detailed spectral modeling,

1. Ten are well fitted with spectral models consistent with accreting X-ray binaries, namely a disk blackbody or a blackbody plus power law. Three of the sources well described with a blackbody plus power law combination have blackbody temperatures at or below 0.1 keV. These are even lower than temperatures inferred from ULX intermediate mass black hole candidates (see, e.g., Miller et al. 2004). The luminosities of these sources also do not indicate the presence of an intermediate mass black hole.

2. In addition, 16 sources are well fitted by a single power law. With one exception, all the photon indices are in the range  $\sim 1-2$ , consistent with Galactic X-ray binaries (Tanaka 2001). The photon indices are not inconsistent with AGNs, but we expect only  $\sim 3$  background AGNs among the bright sources. Two-thirds of the sources well fitted by a single power law are also well fitted by a disk blackbody model with inner disk temperatures in the range 1.0–3.0 keV, which would be consistent with Galactic BH and NS binaries (Tanaka 2001).

3. There are also 4 sources with bremsstrahlung spectra and temperatures between  $\sim 2$  and 7 keV.

Moreover, 12 of 30 sources also show long-term variability, confirming their nature as accreting objects. Therefore, more than half (30) of the sources are consistent with being X-ray binaries based on the X-ray spectrum.

The majority (12) of the remaining 13 sources are well fitted by thermal plasma models (bremsstrahlung or apec models as discussed above), 7 of which with relatively low temperatures around 0.2 keV. Five of these 12 sources are variable. Three sources with unusually low bremsstrahlung temperatures from 0.1 to 0.3 keV are also well fitted by an apec model as well; one

is variable. The *ap*ec temperatures of these sources are around 0.3 keV and abundances are consistent with the overall metallicity of M33 (Blair & Kirshner 1985) (see Fig. 4). A blackbody model does not provide a good fit to the data. Five nonvariable of the 12 sources are coincident with SNRs (Gordon et al. 1999). Variable sources in this category are candidates for quasi-soft sources.

Two sources are well fitted by a single blackbody with temperatures of  $\sim 75$  and  $\sim 37$  eV, respectively. One of the sources is a long-term variable with no significant spectral variability. The other source has been observed only once. Both sources are not significantly detected above 1 keV. These sources are the best candidates for supersoft sources in M33.

Given the spectra, and variability, the majority of these sources are likely X-ray binaries, with a sizable fraction of SNRs/H II regions confirming a young X-ray source population.

*Spectral variability.*—Six of the bright sources show evidence for spectral variability. The type of variability is varied, as has been seen in other galaxies as well (Zezas et al. 2006). The spectral variability is sometimes correlated with luminosity (M33 X-4, X-13), and sometimes not (M33 X-5). In the source X-4 and X-5 the spectral change seems to originate in the column density–photon index degeneracy. In both cases, the thermal component (blackbody or disk blackbody) remains constant, whereas the photon index and column density change their values. With the current data it is not possible to decide whether there is a change in column density within the system or a genuine change in the hard component, assuming that the model is a correct description. M33 X-13 and CXO J013329.0+304216 both show a continuous softening of the spectrum that is correlated in both cases with an increase in luminosity, and they could be identified with quasi-soft sources. The other two sources show significant change only in the soft band with only moderate change in luminosity.

Given the brightness, spectra, and variability (temporal and spectral) these sources are highly likely X-ray binaries.

A comparison of  $N_{\text{H}}$  values measured from the X-ray spectra and H I radio observations of M33 shows that the X-ray absorption is larger for most sources than inferred from H I column density. A few sources have lower X-ray absorption than expected and may be located in front of the H I gas. However, the majority

of sources is intrinsically absorbed. The absorption in X-rays can be compared with values observed in Galactic X-ray binaries and is generally moderate at a few  $10^{21}$  cm $^{-2}$ .

This comparison allows the localization of a few sources in M33 and indicates for most sources intrinsic absorption at the same level as observed in Galactic X-ray binaries.

The luminosity function of M33 sources and optical counterparts from Grimm et al. (2005) have shown that the X-ray source population in M33 is dominated by young objects. The long-term variability, spectra, and spectral variability presented in this paper provide evidence that a large majority of sources are X-ray binaries. The properties of the X-ray binaries (variability, spectral parameters including absorption) are very similar to HMXBs in the Milky Way or the Magellanic Clouds. Thus, X-ray binary populations do not show strong variations over the parameters, e.g., metallicity, covered by the Milky Way, M33, and the Magellanic Clouds. Thus, the M33 X-ray source population confirms our knowledge about HMXB populations in the Milky Way and other galaxies. Therefore, M33 can also be used as a comparison template for similar galaxies at larger distances, which is important as galaxies of this type are numerous.

Comparisons with previous X-ray missions show that repeated observations of a galaxy are important to study the X-ray source population in detail. This analysis also shows that especially with repeat observations it is possible to identify the major parts of an X-ray population on X-ray data alone. The ongoing deep *Chandra* survey of M33 will add significantly more data to such an analysis and provide a more detailed picture of the M33 X-ray source population.

This work has been supported by NASA grant GO2-3135X and by grant AR6-7007X from Chandra X-ray Center operated by the SAO for NASA. This research has made use of the NASA/IPAC Extragalactic Database (NED), which is operated by the Jet Propulsion Laboratory, California Institute of Technology, under contract with the National Aeronautics and Space Administration. We thank the referee for constructive comments on the paper.

*Facilities:* CXO

## APPENDIX A

### TIME VARIABILITY

Table 2 presents the analysis results of variability between observations. We use Poissonian statistics for the background-subtracted source counts. The table shows only sources with variability above  $3\sigma$  between any two observations. The first column gives the name of the source, the next three columns give the fluxes, with errors in parentheses, for each observation if the source was detected, or  $3\sigma$  upper limits on the flux. The last three columns give the significance of variability between any two observations. Comparisons between upper limits are set to zero.

## APPENDIX B

### SPECTRA

The spectra are combined in one plot (see Fig. Set 9 and Table 3). Black corresponds to the first observation, red to a second observation, and green to a third observation. For easier comparison contour plots are also overlaid for all observations. Solid contours correspond to the first observation, dashed contours to the second observation, and dotted to the third observation. Note that not all sources are observed in all observations.

Some sources are well fitted by a bremsstrahlung model with low temperatures. We also fit these spectra with an *ap*ec model, which also provides a good fit. In case the *ap*ec model provides a good fit as well, we give the parameters and contour plots in the table and figures.

TABLE 2  
LIST OF SOURCES VARIABLE AT MORE THAN  $3\sigma$  BETWEEN ANY OBSERVATIONS

SOURCE	FLUX ( $10^{-7}$ counts $s^{-1}$ $cm^{-2}$ )			SIGNIFICANCE ( $\sigma$ )		
	1730	786	2023	1730→786	786→2023	1730→2023
CXO J013308.3+304802.....	...	66 (8.4)	<4.5	...	7.3	...
CXO J013315.1+305317.....	...	3000 (46)	5800 (62)	...	36.3	...
CXO J013315.5+304448.....	180 (18)	170 (19)	<4.3	0.4	8.7	9.8
CXO J013321.7+303858.....	24 (5.2)	...	<6.2	...	...	3.4
CXO J013321.9+303921.....	22 (5.0)	...	<4.3	...	...	3.5
CXO J013323.9+304821.....	...	46 (7.4)	<9.2	...	5.0	...
CXO J013324.4+304401.....	1700 (39)	2800 (45)	2500 (31)	18.5	5.5	16.1
CXO J013327.7+304645.....	14 (4.3)	20 (5.4)	52 (6.6)	0.9	3.8	4.8
CXO J013328.6+304321.....	20 (4.7)	19 (4.9)	<3.5	0.1	3.2	3.5
CXO J013329.0+304216.....	150 (12)	160 (11)	200 (10)	0.6	2.7	3.2
CXO J013329.2+304537.....	34 (6.0)	39 (6.5)	<6.2	0.6	5.0	4.6
CXO J013329.2+304508.....	140 (11)	170 (12)	120 (8.2)	1.8	3.4	1.5
CXO J013333.0+304920.....	...	28	<6.8	...	3.5	...
CXO J013334.1+303714.....	43 (6.4)	...	<4.3	...	...	6.0
CXO J013335.5+303728.....	12 (4.0)	19 (3.7)	<4.3	1.3	4.0	1.9
CXO J013336.3+303742.....	90 (9.1)	48 (5.5)	<7.3	3.9	7.4	9.1
CXO J013337.4+304718.....	71 (8.4)	100 (9.7)	29 (5.2)	2.3	6.5	4.3
CXO J013339.2+304049.....	50 (6.7)	47 (8.4)	<6.2	0.3	4.9	6.5
CXO J013340.0+304323.....	32 (5.6)	23 (4.7)	<9.5	1.2	2.9	4.0
CXO J013341.5+304136.....	26 (5.0)	37 (5.6)	<10.7	1.5	4.7	3.1
CXO J013341.8+303848.....	70	150	200	6.8	3.8	10.4
CXO J013342.5+304253.....	15 (4.2)	56 (6.8)	<11.8	5.1	6.5	0.8
CXO J013343.4+304630.....	20 (8.8)	61 (7.7)	79 (7.5)	3.5	1.7	5.1
CXO J013344.2+304026.....	12	30.8	<5	2.3	3.9	1.5
CXO J013346.2+303807.....	<3.5	<4.3	90 (9.0)	0.0	9.5	9.6
CXO J013350.5+303821.....	27 (5.1)	57 (5.7)	<11.8	3.9	7.9	3.0
CXO J013353.6+303605.....	<10.4	9.9 (2.9)	...	0.2	...	...
CXO J013354.8+303309.....	120 (10)	230 (12)	...	7.0	...	...
CXO J013356.8+303729.....	37 (8.4)	83 (6.7)	...	4.3	...	...
CXO J013358.8+305004.....	...	93 (9.8)	36 (4.5)	...	5.3	...
CXO J013409.8+305044.....	...	3.8	33 (4.5)	...	5.3	...
CXO J013410.3+305346.....	...	<5	23 (3.8)	...	4.7	...
CXO J013410.5+303946.....	72 (7.9)	120 (8.0)	120 (7.7)	4.3	0.0	4.4
CXO J013416.7+305101.....	...	<7.7	27 (3.7)	...	5.2	...
CXO J013419.2+304942.....	...	<5	17 (3.0)	...	4.0	...
CXO J013424.6+304428.....	<5.1	26 (6.0)	<6.8	3.5	3.2	0.0
CXO J013425.3+304157.....	<15.2	33 (6.2)	11 (2.9)	2.9	3.2	1.4
CXO J013426.7+304811.....	...	<3.5	14 (2.8)	...	3.8	...
CXO J013429.1+304212.....	13 (4.5)	<14.7	7.5 (2.2)	0.4	3.3	1.1
CXO J013429.7+305026.....	...	<7.7	34 (3.9)	...	6.7	...
CXO J013432.1+305158.....	...	<5	93 (13)	...	6.8	...
CXO J013432.5+305035.....	...	<5	15 (3.0)	...	3.3	...
CXO J013432.7+303436.....	51 (8.3)	<3.6	...	5.7	...	...
CXO J013433.7+304701.....	...	430 (27)	280 (14)	...	4.9	...
CXO J013435.0+304439.....	...	<7.7	17 (3.0)	...	3.1	...
CXO J013436.4+304713.....	...	50.3	23 (3.3)	...	3.1	...
CXO J013446.7+304449.....	...	<6.4	21 (3.3)	...	4.4	...
CXO J013449.0+304446.....	...	<6.4	34 (4.0)	...	6.9	...
CXO J013451.1+304356.....	...	<3.5	30 (3.8)	...	7.0	...
CXO J013451.9+304615.....	...	120 (14)	48 (4.8)	...	4.9	...

NOTE.—Comparisons between upper limits are set to zero.

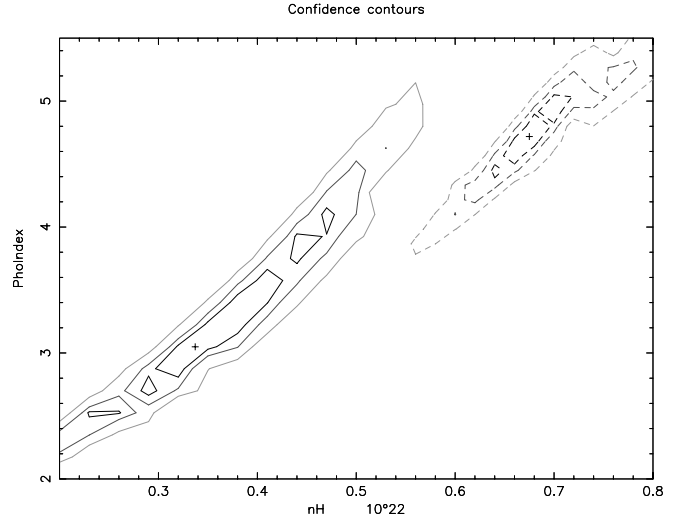
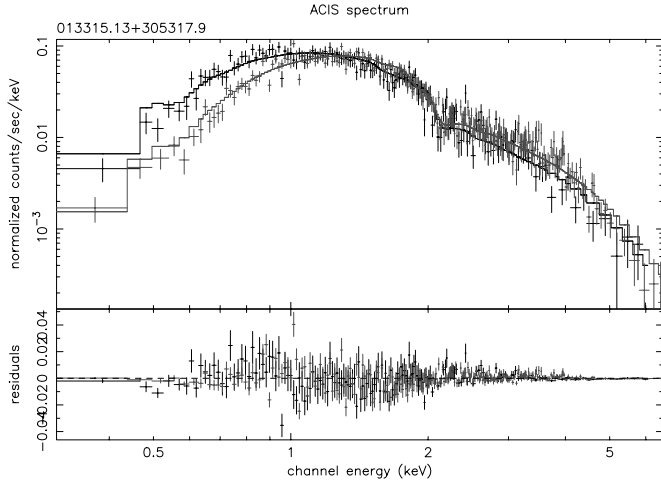


FIG. SET 9.—Spectrum and contour example for CXO J013315.1+305317. Models and parameters are shown in Table 3. [See the electronic edition of the Supplement for a color versions of Figs. 9.1–9.26.]

TABLE 3  
SPECTRAL PARAMETERS

Source	ObsID	XSPEC Model	$N_{\text{H}}$ ( $10^{22} \text{ cm}^{-2}$ )	$kT$ , $T_0$ , $T_{\text{in}}$ , $E$ , $\sigma$ (keV), $Z$ (Solar Abund.)
CXO J013253.4+303817 (M33 X-1).....	1730	bremss	$0.05^{+0.04}_{-0.03}$	$kT = 7.1^{+3.55}_{-2.0}$
CXO J013253.9+303312 (M33 X-2).....	1730	pow	$0.16^{+0.07}_{-0.05}$	$\Gamma = 1.9^{+0.26}_{-0.33}$
CXO J013308.3+304802.....	786	bremss	$0.17^{+0.12}_{-0.09}$	$kT = 2.3^{+4.3}_{-1.2}$
CXO J013315.1+305317 (M33 X-4).....	786	bbbody + pow	$0.34^{+0.05}_{-0.13}$	$kT = 0.62^{+0.07}_{-0.11}$ $\Gamma = 3.0^{+0.3}_{-0.7}$
	2023	bbbody + pow	$0.67^{+0.12}_{-0.09}$	$kT = 0.69 \pm 0.04$ $\Gamma = 4.7^{+0.75}_{-0.25}$
CXO J013315.5+304448.....	1730	pow	$0.31^{+0.26}_{-0.18}$	$\Gamma = 2.7^{+0.75}_{-0.65}$
	786	pow	$1.43^{+1.02}_{-0.63}$	$\Gamma = 5.8^{+2.7}_{-1.75}$
CXO J013324.4+304401 (M33 X-5).....	1730	diskbb + pow	$<0.56$	$T_{\text{in}} = 1.3^{+0.15}_{-0.11}$ $\Gamma = 9.5^a$
	786	diskbb + pow	$0.64^{+0.24}_{-0.32}$	$T_{\text{in}} = 1.3^{+0.23}_{-0.1}$ $\Gamma = 5.7^{+1.3}_{-1.9}$
	2023	diskbb + pow	$0.28^{+0.28}_{-0.2}$	$T_{\text{in}} = 1.4^{+0.13}_{-0.2}$ $\Gamma = 3.5^{+1.9}_{-0.9}$
CXO J013327.7+304645.....	2023	bbbody + pow	$<0.33$	$kT = 1.2^a$ $\Gamma = 3.0^{+1.7}_{-1.4}$
CXO J013329.0+304216.....	1730	bremss	$0.34^{+0.18}_{-0.1}$	$kT = 0.23^{+0.04}_{-0.08}$
	786	bremss	$0.37^{+0.44}_{-0.01}$	$kT = 0.20^{+0.01}_{-0.09}$
	2023	bremss	$0.55^{+0.04}_{-0.01}$	$kT = 0.16^{+0.01}_{-0.01}$
	1730	apec	$<0.31$	$kT = 0.36^{+0.3}_{-0.1}$ $Z = 0.11^{+0.19}_{-0.07}$
	786	apec	$<0.16$	$kT = 0.4^{+0.14}_{-0.06}$ $Z = 0.22^{+0.34}_{-0.12}$
	2023	apec	$0.25^{+0.15}_{-0.1}$	$kT = 0.28 \pm 0.05$ $Z = 0.22^{+2.2}_{-0.13}$
CXO J013329.3+304508.....	1730	apec	$0.14^{+0.1}_{-0.09}$	$kT = 4.7^{+5.9}_{-1.4}$ $Z < 4.5$
	786	apec	$<0.13$	$kT = 8.2^{+16.8}_{-4.3}$ $Z < 1.9$
	2023	apec	$<0.09$	$kT = 17.2^{>\infty}_{-10.2}$ $Z = 2.0^a$
CXO J013329.4+304912.....	786	bremss	$0.49^{+0.51}_{-0.34}$	$kT = 0.15^{+0.09}_{-0.07}$
	2023	bremss	$0.37^{+0.08}_{-0.02}$	$kT = 0.2^{+0.08}_{-0.01}$
	786	apec	$<0.31$	$kT = 0.31^{+0.18}_{-0.1}$ $Z = 0.3^{+2.2}_{-0.26}$
	2023	apec	$<0.6$	$kT = 0.26^{+0.37}_{-0.13}$ $Z = 0.05^{+0.23}_{-0.04}$
CXO J013331.1+303333 (M33 X-14).....	1730	bremss	$0.17^{+0.06}_{-0.05}$	$kT = 0.29^{+0.05}_{-0.03}$ $E_{1/2} = 0.89^{+0.03}_{-0.03}$ $\sigma_{1/2} < 0.045$
		+2*gauss		$E_{1/2} = 1.35^{+0.02}_{-0.02}$ $\sigma_{1/2} < 0.035$
CXO J013334.1+303210 (M33 X-7).....	1730	diskbb	$<0.05$	$T_{\text{in}} = 1.0^{+0.05}_{-0.03}$
CXO J013335.9+303627.....	1730	bremss	$0.22^{+0.29}_{-0.16}$	$kT = 0.31^{+0.17}_{-0.12}$
	1730	apec	$<0.38$	$kT = 0.40^{+0.28}_{-0.12}$ $Z = 0.12^{+0.55}_{-0.09}$
CXO J013336.3+303742.....	1730	pow	$0.62^{+0.4}_{-0.33}$	$\Gamma = 2.1^{+0.9}_{-0.8}$
	786	pow	$0.25^{+0.3}_{-0.22}$	$\Gamma = 1.2^{+0.85}_{-0.75}$
CXO J013337.4+304718.....	1730	pow	$<0.33$	$\Gamma = 1.9^{+0.65}_{-0.55}$
	786	pow	$0.22^{+0.17}_{-0.15}$	$\Gamma = 2.0^{+0.55}_{-0.45}$
	2023	pow	$<0.49$	$\Gamma = 0.8^{+0.7}_{-0.55}$
CXO J013341.8+303848.....	1730	apec	$<0.07$	$kT = 0.70 \pm 0.15$ $Z = 0.17^{+0.19}_{-0.12}$
	786	apec	$<0.05$	$kT = 0.70^{+0.09}_{-0.12}$ $Z = 0.12^{+0.07}_{-0.06}$
	2023	apec	$<0.07$	$kT = 0.72^{+0.17}_{-0.15}$ $Z < 0.04$
CXO J013343.4+304630.....	1730	bbbody	$0.79^b$	$kT = 0.07^b$
	786	bbbody	$0.79^{+0.32}_{-0.44}$	$kT = 0.07^{+0.035}_{-0.005}$
	2023	bbbody	$0.83^{+0.52}_{-0.08}$	$kT = 0.08^{+0.005}_{-0.055}$
CXO J013346.2+303807.....	2023	bbbody + apec	$0.06^b$	$kT = 0.02 \pm 0.01$ $kT = 3.1^{+7.3}_{-1.5}$ $Z = 0.3^b$

TABLE 3—Continued

Source	ObsID	XSPEC Model	$N_{\text{H}}$ ( $10^{22} \text{ cm}^{-2}$ )	$kT$ , $T_0$ , $T_{\text{in}}$ , $E$ , $\sigma$ (keV), $Z$ (Solar Abund.)			
CXO J013346.5+303748	1730	pow	<0.14	$\Gamma = 1.6 \pm 0.35$			
	786	pow	$0.1^{+0.1}_{-0.08}$	$\Gamma = 1.1^{+0.35}_{-0.25}$			
CXO J013350.5+303821	1730	pow	<0.39	$\Gamma = 1.6^{+0.9}_{-0.7}$			
	786	pow	<0.16	$\Gamma = 1.5^{+0.4}_{-0.4}$			
CXO J013354.8+303309 (M33 X-13)	1730	brems	$0.30^{+0.27}_{-0.12}$	$kT = 0.22^{+0.07}_{-0.07}$			
	786	brems	$0.36^{+0.15}_{-0.11}$	$kT = 0.18^{+0.04}_{-0.05}$			
CXO J013356.8+303729	1730	pow	$0.15^{\text{b}}$	$\Gamma = 1.5^{\text{b}}$			
	786	pow	$0.15^{+0.1}_{-0.09}$	$\Gamma = 1.5^{+0.4}_{-0.35}$			
CXO J013358.8+305004 (M33 X-9a)	786	pow	<0.46	$\Gamma = 1.7^{+0.2}_{-0.8}$			
	2023	pow	$0.54^{+0.22}_{-0.45}$	$\Gamma = 1.8^{+0.5}_{-0.7}$			
CXO J013401.5+303136	786	apec + pow	$0.94^{+0.5}_{-0.54}$	$kT = 6.3^{\text{a}}$	$Z = 0.3^{\text{b}}$	$\Gamma = 3.4^{+5.2}_{-1.3}$	
CXO J013402.0+303004	786	bbody + pow	<0.27	$kT = 0.04^{+0.025}_{-0.01}$	$\Gamma = 1.8^{+0.85}_{-0.35}$		
CXO J013409.9+303219	786	bbody	$0.73^{+0.34}_{-0.25}$	$kT = 0.037^{+0.007}_{-0.006}$			
CXO J013410.5+303946	1730	diskbb	$0.06^{\text{b}}$	$T_{\text{in}} = 1.2^{+0.4}_{-0.3}$			
	786	pow	$0.06^{\text{b}}$	$\Gamma = 1.7 \pm 0.1$			
	2023	diskbb	$0.06^{\text{b}}$	$T_{\text{in}} = 1.2 \pm 0.2$			
CXO J013410.6+304223	1730	brems	$0.79^{+0.51}_{-0.43}$	$kT = 0.11^{+0.07}_{-0.03}$			
	2023	brems	<0.19	$kT = 0.3^{+0.07}_{-0.05}$			
CXO J013421.2+304932	2023	diskbb	$1.17^{+0.55}_{-0.48}$	$T_{\text{in}} = 1.7^{+1.7}_{-0.5}$			
CXO J013425.4+302821	786	bknpow	<0.25	$\Gamma_1 = 2.9^{+1.6}_{-1.1}$	$E_{\text{break}} > 1.2$	$\Gamma_2 = 0.16^{+2.1}_{-1.0}$	
CXO J013425.5+305514	786	pow	$0.16^{+0.07}_{-0.06}$	$\Gamma = 2.1^{+0.25}_{-0.15}$			
	2023	pow	$0.17^{+0.03}_{-0.04}$	$\Gamma = 2.0^{+0.14}_{-0.04}$			
CXO J013427.0+304314	786	pow	<0.27	$\Gamma = 0.9^{+1.6}_{-0.3}$			
	2023	pow	<0.17	$\Gamma = 1.7^{+0.6}_{-0.3}$			
CXO J013432.0+303455	1730	brems	$2.7^{+0.8}_{-1.1}$	$kT = 2.7^{+11.3}_{-0.9}$			
CXO J013433.7+304701	786	bbody + pow	<0.9	$kT = 0.1 \pm 0.03$			
	2023	bbody + pow	$0.46^{+0.54}_{-0.33}$	$kT = 0.09^{+0.05}_{-0.04}$			
CXO J013435.1+305646	2023	brems	$1.1^{+0.36}_{-0.38}$	$kT = 4.7^{+5.5}_{-2.4}$			
CXO J013438.8+304538	786	pow	<0.18	$\Gamma = 1.6^{+0.65}_{-0.35}$			
	2023	pow	<0.17	$\Gamma = 1.8^{+0.4}_{-0.3}$			
CXO J013438.8+305504	2023	pow	$0.06 \pm 0.04$	$\Gamma = 1.9^{+0.1}_{-0.12}$			
CXO J013439.8+305143	2023	pow	<0.2	$\Gamma = 1.5^{+0.5}_{-0.3}$			
CXO J013444.5+304922	786	diskbb	<0.07	$T_{\text{in}} = 2.7^{+25}_{-1.7}$			
	2023	diskbb	<0.08	$T_{\text{in}} = 0.46^{+0.09}_{-0.07}$			
CXO J013444.6+305535	2023	bbody + pow	$0.15^{+0.1}_{-0.04}$	$kT = 0.03^{\text{a}}$			
CXO J013451.9+304615	786	pow	$0.06^{\text{b}}$	$\Gamma = 1.1^{+0.35}_{-0.4}$			
	2023	pow	$0.06^{\text{b}}$	$\Gamma = 1.7^{+0.27}_{-0.35}$			
CXO J013453.2+305718	2023	pow	$0.27^{+0.29}_{-0.23}$	$\Gamma = 2.1^{+0.8}_{-0.7}$			
CXO J013501.1+304345	786	pow	<0.54	$\Gamma = 1.8^{+1.3}_{-0.5}$			
	2023	pow	<0.25	$\Gamma = 1.9^{+0.4}_{-0.5}$			

<sup>a</sup> Parameter unconstrained at 90% CL.<sup>b</sup> Parameter fixed.

## REFERENCES

- Alexander, D. M., et al. 2003, *AJ*, 126, 539  
Blair, W. P., & Kirshner, R. P. 1985, *ApJ*, 289, 582  
Bradshaw, C. F., Geldzahler, B. J., & Fomalont, E. B. 2003, *ApJ*, 592, 486  
Cash, W. 1979, *ApJ*, 228, 939  
Condon, J. J. 1987, *ApJS*, 65, 485  
Di Stefano, R., & Kong, A. K. H. 2004, *ApJ*, 609, 710  
Freedman, W. L., Wilson, C. D., & Madore, B. F. 1991, *ApJ*, 372, 455  
Gierliński, M., & Done, C. 2004, *MNRAS*, 347, 885  
Gordon, S. M., Duric, N., Kirshner, R. P., Goss, W. M., & Viallefond, F. 1999, *ApJS*, 120, 247  
Grimm, H.-J., McDowell, J., Zezas, A., Kim, D.-W., & Fabbiano, G. 2005, *ApJS*, 161, 271  
Hippelstein, H., Haas, M., Tuffs, R. J., Lemke, D., Stickel, M., Klaas, U., & Völkel, H. J. 2003, *A&A*, 407, 137  
Jenkins, L. P., Roberts, T. P., Warwick, R. S., Kilgard, R. E., & Ward, M. J. 2005, *MNRAS*, 357, 401  
Kahabka, P., & van den Heuvel, E. P. J. 1997, *ARA&A*, 35, 69  
Kahn, S. M., Seward, F. D., & Chlebowski, T. 1984, *ApJ*, 283, 286  
Kim, D.-W., et al. 2004, *ApJS*, 150, 19  
Kraft, R. P., Burrows, D. N., & Nousek, J. A. 1991, *ApJ*, 374, 344  
Kubota, A., & Done, C. 2004, *MNRAS*, 353, 980  
Kuulkers, E., Norton, A., Schwope, A., & Warner, B. 2006, in *Compact Stellar X-Ray Sources*, ed. W. Lewin & M. van der Klis (Cambridge: Cambridge Univ. Press), 421  
Liu, Q. Z., van Paradijs, J., & van den Heuvel, E. P. J. 2000, *A&AS*, 147, 25  
———. 2001, *A&A*, 368, 1021  
Long, K. S., Charles, P. A., Blair, W. P., & Gordon, S. M. 1996, *ApJ*, 466, 750  
Maccarone, T. J. 2003, *A&A*, 409, 697  
Markert, T. H., & Rallis, A. D. 1983, *ApJ*, 275, 571  
McClintock, J., & Remillard, R. 2006, in *Compact Stellar X-Ray Sources*, ed. W. Lewin & M. van der Klis (Cambridge: Cambridge Univ. Press), 157  
Miller, J. M., Fabian, A. C., & Miller, M. C. 2004, *ApJ*, 614, L117  
Mushotzky, R. F., Done, C., & Pounds, K. A. 1993, *ARA&A*, 31, 717  
Okada, Y., Takahashi, H., & Makishima, K. 2001, *PASJ*, 53, 663  
Paolillo, M., Schreier, E. J., Giacconi, R., Koekemoer, A. M., & Grogin, N. A. 2004, *ApJ*, 611, 93  
Parmar, A. N., et al. 2001, *A&A*, 368, 420  
Pietsch, W., Haberl, F., Sasaki, M., Gaetz, T. J., Plucinsky, P. P., Ghavamian, P., Long, K. S., & Pannuti, T. G. 2006, *ApJ*, 646, 420  
Pietsch, W., Mochejska, B. J., Misanovic, Z., Haberl, F., Ehle, M., & Trinchieri, G. 2004, *A&A*, 413, 879  
Predehl, P., & Schmitt, J. H. M. M. 1995, *A&A*, 293, 889

- Prestwich, A. H., Irwin, J. A., Kilgard, R. E., Krauss, M. I., Zezas, A., Primini, F., Kaaret, P., & Boroson, B. 2003, *ApJ*, 595, 719
- Scargle, J. D. 1998, *ApJ*, 504, 405
- Schulman, E., & Bregman, J. N. 1995, *ApJ*, 441, 568
- Sivakoff, G. R., Sarazin, C. L., & Jordán, A. 2005, *ApJ*, 624, L17
- Stark, A. A., Gammie, C. F., Wilson, R. W., Bally, J., Linke, R. A., Heiles, C., & Hurwitz, M. 1992, *ApJS*, 79, 77
- Tanaka, Y. 2001, in *Black Holes in Binaries and Galactic Nuclei*, ed. L. Kaper, E. P. J. van den Heuvel, & P. A. Woudt (Berlin: Springer), 141
- Trinchieri, G., Fabbiano, G., & Peres, G. 1988, *ApJ*, 325, 531
- van der Klis, M. 2006, *Compact Stellar X-Ray Sources*, ed. W. H. Lewin & M. van der Klis (Cambridge: Cambridge Univ. Press), 39
- Vrtilek, S. D., McClintock, J. E., Seward, F. D., Kahn, S. M., & Wargelin, B. J. 1991, *ApJS*, 76, 1127
- Zezas, A., Fabbiano, G., Baldi, A., Schweizer, F., King, A. R., Ponman, T. J., & Rots, A. H. 2006, *ApJS*, 166, 211

*Note added in proof.*—After acceptance of this paper, it has come to our attention that Misanovic et al. (*A&A*, 448, 1247 [2006]) have analyzed variability data for M33 based on *XMM-Newton* data, and that Hatzidimitriou et al. (*A&A*, 451, 835 [2006]) identify CXO J013343.4+304630 as a foreground star.